4th IAA Planetary Defense Conference – PDC 2015
13-17 April 2015, Frascati, Roma, Italy

IAA-PDC-15-03-15

GPU-ACCELERATED COMPUTATIONAL TOOL DEVELOPMENT FOR STUDYING THE EFFECTIVENESS OF NUCLEAR SUBSURFACE EXPLOSIONS

Ben J. Zimmerman[a,1,*], Bong Wie[a,2,*]

[a]Iowa State University, 2271 Howe Hall, Ames, IA 50011-2271, USA

Abstract

This paper is concerned with the development of a new GPU (Graphics Processing Units) accelerated computational tool for validating the effectiveness of a hypervelocity kinetic impact and a subsequent nuclear subsurface explosion. Accurate prediction of energy coupling with the target asteroid body is crucial for asteroid disruption, In this paper, we present numerical solutions of asteroid disruption techniques via high-order numerical methods. All simulations are conducted using GPUs. High-order methods have a computationally efficient framework, well suited for the GPU architecture, allowing simulations to be performed orders of magnitude faster than the Central Processing Unit (CPU) counterpart. Several hypervelocity kinetic impact problems are simulated and compared to each other. In the simulations, the mass, shape, and number of kinetic impactors are varied to cover a wide variety of mission scenarios. Similar to a rectangle shape impactor (with $L > D$) that generates a deeper crater than a box-shaped impactor, multiple impactors in series striking in sequence also generate a deeper crater. It is also found that simultaneous parallel impacts across the target's surface can cause more effective pulverization of the target asteroid. A nuclear subsurface explosion following multiple kinetic impactors in series was also simulated to examine its overall effectiveness for pulverizing the target asteroid.

Keywords: kinetic impact, multiple impactors in series or parallel, asteroid disruption/pulverization, nuclear subsurface explosions, GPU CUDA, HAIV

1. INTRODUCTION

The successful mitigation of near-Earth objects (NEOs) is a growing concern, which was spurred by Chelyabinsk event (caused by a 17-m meteor) in Russia on February 15, 2013 and a near miss by asteroid 2012 DA_{14} (~30 m diameter), both which occurred on the same day. Most methods proposed previously for asteroid mitigation require a substantial mission lead time for deflection. While these methods are appealing, they simply cannot handle short warning cases. The best proposed method, described in a report by the United States National Research Council (NRC), suggests the use of a nuclear explosive device (NED) for immediate threats [1]. If a small amount of energy from the device is actually coupled to the asteroid body, non-ideal fragmentation/pulverization of the target NEO can occur [2]. One solution to avoiding such undesirable situation is to employ a subsurface explosion, which

[*]Corresponding author
Email addresses: bzimmer@iastate.edu (Ben J. Zimmerman), bongwie@iastate.edu (Bong Wie)
[1]Graduate Research Assistant, Asteroid Deflection Research Center, Department of Aerospace Engineering
[2]Vance Coffman Endowed Chair Professor, Asteroid Deflection Research Center, Department of Aerospace Engineering

can transfer a significant amount of energy to the target body. The concept of blending a hypervelocity kinetic impactor with a subsurface nuclear explosion was investigated in a NASA Innovative Advanced Concepts (NIAC) study, resulting in a Hypervelocity Asteroid Intercept Vehicle (HAIV) mission concept [3, 4, 5, 6]. The HAIV concept uses a hypervelocity impactor to generate an initial crater and a follower vehicle, which carries an NED. The follower enters the crater and the NED is detonated, emulating a subsurface nuclear explosion. The benefit of subsurface nuclear explosions has been examined in an NRC report [7]. Depending on the amount of energy emitted from the NED along with its buried depth, it can be up to 20 times more efficient at coupling energy to the system when compared to a surface explosion. In our previous work, a factor of 10 has been observed [8].

This paper is focused on the lead kinetic impactor and its effect on the target body. The crater generated by the impactor must be deep enough to couple a significant amount of energy from the nuclear blast. If the crater is too shallow, then the subsurface explosion will behave similar to that of a contact burst and large amounts of energy from the NED will be lost in surrounding space, or escape through the crater. The generated crater does depend on the target's density and overall shape, and this study only considers a single, circular target, with constant density (no porosity is considered).

In addition to the HAIV concept, non-nuclear options are also of interest. The kinetic energy imparted to the target from kinetic impactors is monitored for several cases, to determine if disruption via kinetic impact only is feasible for small asteroids. We consider various cases with single and multiple kinetic impactors in this paper. The single impactor is of high density and mass, while the sum of the multiple impactor's masses is equivalent to the single large impactor mass. Two different multiple impactor configurations are studied. The first case illustrates an array of impactors, which strike the target surface in parallel. The second case shows an array impactors in series. The goal of this research is to determine which case is more effective for asteroid disruption. Both the coupled kinetic energy to the target and density contours are studied to this end.

Numerical simulation of this problem requires high resolution and large computational power. To accomplish this, we apply high-order numerical methods with Graphics Processing Units (GPUs). The solver is the same used in [8], with extension to the discontinuous Galerkin method [9, 10, 11] for improved accuracy in simulations. NVIDIA's Compute Unified Device Rrchitecture (CUDA) is used to hasten the solution generation, and arrive at the final required time by orders of magnitude faster than CPU simulations. The application of high-order methods with GPU CUDA has already been investigated in [12, 13], where significant increases in computing speed has been observed. Since our research group does not have access to a large computational CPU cluster, CUDA is of high interest. Numerical modeling of the hypervelocity kinetic impact and following nuclear explosion is conducted with the two-dimensional Euler equations. Upon impact, the pressure imparted by the impactor and much greater than the target materials strength, hence the material behaves like a compressible fluid [14]. The equations are solved in an Eulerian framework, and the stiffened equation of state is implemented for the impactor and asteroid target. The stiffened equation of state is not sufficient enough for the problem to be solved, as the pressures, energy densities, and temperatures are so incredibly high that the equation of state implemented does not properly define the materials. Therefore, more accurate equations of states will be considered in future work.

This paper is organized as follows: Section 1describes the mathematical modeling of the problem, including the governing equations, the equation of state, and the numerical method. Section 2 describes the problem in detail, outlining several test cases to be discussed. Section 3 shows results for cases of multiple kinetic impactors and preliminary validation results for the HAIV concept. Finally, Section 4 presents conclusions and future work.

2. NUMERICAL MODELING

This section outlines the mathematical model used in the simulations. The governing equations and numerical discretization are outlined. Additionally, a one-dimensional problem is simulated to show proper implementation of the model.

2.1. Governing Equations

As mentioned previously, the velocity is extremely high in hypervelocity problems, such that most materials behave similar to fluids. The two-dimensional Euler equations are chosen for numerical modeling, and are governed by conservation of mass, momentum, and energy, as follows:

$$\frac{\partial \rho}{\partial t} + \frac{\partial (\rho u)}{\partial x} + \frac{\partial (\rho v)}{\partial y} = 0 \tag{1}$$

$$\frac{\partial \rho u}{\partial t} + \frac{\partial \left(\rho u^2 + p\right)}{\partial x} + \frac{\partial (\rho u v)}{\partial y} = 0 \tag{2}$$

$$\frac{\partial \rho v}{\partial t} + \frac{\partial (\rho u v)}{\partial x} + \frac{\partial \left(\rho v^2 + p\right)}{\partial y} = 0 \tag{3}$$

$$\frac{\partial e}{\partial t} + \frac{\partial \left[u(e+p)\right]}{\partial x} + \frac{\partial \left[v(e+p)\right]}{\partial y} = 0 \tag{4}$$

In Equations (1) - (4), ρ is the density, u is the x-direction velocity, v is the y-direction velocity, p is the pressure, and e is the total energy per unit volume. To close the system, an appropriate equation of state must be defined. For this study, a stiffened equation of state is considered as

$$p = \rho e(\gamma - 1) - \gamma p_o \tag{5}$$

Here, γ is the ratio of specific heats and p_o is a pressure constant. Both γ and p_o depend on the material to be modeled, and can be found via experiments and empirical curve fitting [15]. The speed of sound in the stiffened equation of state model is given as follows:

$$c = \sqrt{\frac{\gamma(p + p_o)}{\rho}} \tag{6}$$

If p_o is set to 0, the stiffened equation of state reduces to the ideal gas equation of state. However, simply defining a new equation of state is not sufficient. Our solver uses an Eulerian framework, and we must track the γ and p_o variables. Similar work for the stiffened equation of state was completed in [16]. The equation of state is integrated into the state variables, further complicating the method and increasing the computational cost of the approach. Two additional state equations are added to the governing model. One equation tracks only the γ term as

$$\frac{\partial}{\partial t}\left(\frac{1}{\gamma - 1}\right) + \frac{\partial}{\partial x}\left(\frac{u}{\gamma - 1}\right) + \frac{\partial}{\partial y}\left(\frac{v}{\gamma - 1}\right) = 0, \tag{7}$$

And the other equation tracks the p_o term as

$$\frac{\partial}{\partial t}\left(\frac{\gamma p_o}{\gamma - 1}\right) + \frac{\partial}{\partial x}\left(\frac{u\gamma p_o}{\gamma - 1}\right) + \frac{\partial}{\partial y}\left(\frac{v\gamma p_o}{\gamma - 1}\right) = 0 \tag{8}$$

The governing equations can be written in the form of a hyperbolic equation as

$$\frac{\partial \boldsymbol{q}}{\partial t} + \vec{\nabla} \cdot \vec{\boldsymbol{F}}(\boldsymbol{q}) = 0 \tag{9}$$

where $\vec{\nabla} \cdot \vec{\boldsymbol{F}}(\boldsymbol{q}) = \dfrac{\partial \boldsymbol{f}(\boldsymbol{q})}{\partial x} + \dfrac{\partial \boldsymbol{g}(\boldsymbol{q})}{\partial y}$. where $\boldsymbol{q}$ is the state variable vector and $\boldsymbol{f}$ and $\boldsymbol{g}$ are flux vectors defined as

$$\boldsymbol{q} = \begin{bmatrix} \rho \\ \rho u \\ \rho v \\ e \\ \dfrac{1}{\gamma - 1} \\ \dfrac{\gamma p_o}{\gamma - 1} \end{bmatrix}, \qquad \boldsymbol{f}(\boldsymbol{q}) = \begin{bmatrix} \rho u \\ p + \rho u^2 \\ \rho u v \\ u(e + p) \\ \dfrac{u}{\gamma - 1} \\ \dfrac{u\gamma p_o}{\gamma - 1} \end{bmatrix}, \qquad \boldsymbol{g}(\boldsymbol{q}) = \begin{bmatrix} \rho v \\ \rho u v \\ p + \rho v^2 \\ v(e + p) \\ \dfrac{u}{\gamma - 1} \\ \dfrac{v\gamma p_o}{\gamma - 1} \end{bmatrix} \tag{10}$$

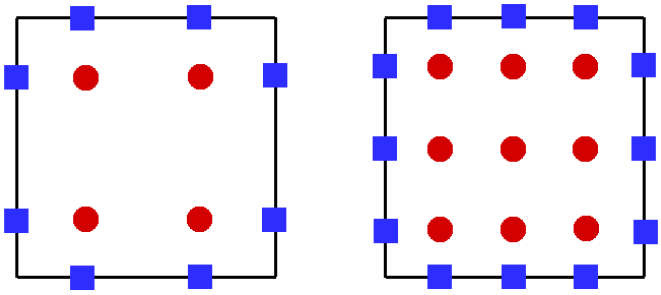

Figure 1: Solution points (circles) and interpolation points (squares) for P^1 and P^2 DG.

Now, the solver can track the interfaces of different fluids/materials throughout the domain. With the governing equations defined, we must discretize the equations with an appropriate method. The discontinuous Galerkin method is chosen for implementation, and is briefly discussed next.

2.2. Numerical Method

The computational domain is discretized with non-overlapping quadrilateral elements. Each element has index i and volume V_i. The elements are transformed into standard elements [17], where a set of solution points and flux points are defined. Figure 1 illustrates the locations of solution points and flux points in a quadrilateral element. The solution points contain the state variable information, while the flux points provide coupling across elements. The number of solution points within an element can be increased, providing a higher order interpolation polynomial and improving accuracy of the method. The figure demonstrates a second order scheme (left element) and a third order scheme (right element). Every element in the domain is discretized with the same number of points, maintaining a constant order of accuracy.

Equation (9) is integrated over an elements volume and multiplied by an arbitrary weighting function w as follows:

$$\int_{V_i} \left[\frac{\partial \boldsymbol{q}}{\partial t} + \vec{\nabla} \cdot \vec{\boldsymbol{F}}(\boldsymbol{q}) \right] w dV = 0 \tag{11}$$

By integrating by parts, approximating $\boldsymbol{q}$ on each element by $\boldsymbol{q}_i$, and using polynomials P^k, we rewrite Equation (11) as

$$\int_{V_i} \frac{\partial \boldsymbol{q}_i}{\partial t} w dV + \int_{\partial V_i} w \vec{\boldsymbol{F}}(\boldsymbol{q}_i) \cdot \boldsymbol{n} dS - \int_{V_i} \vec{\nabla} w \cdot \vec{\boldsymbol{F}}(\boldsymbol{q}_i) dV = 0 \tag{12}$$

The solution and flux polynomial is approximated over the $k+1$ Gauss-Legendre points in each element, as follows:

$$\boldsymbol{q}_i = \sum_{j=1}^{k+1} \boldsymbol{q}_{i,j} \phi_j, \quad \vec{\boldsymbol{F}}(\boldsymbol{q}_{i,j}) = \sum_{j=1}^{k+1} \vec{\boldsymbol{F}}_{i,j} \phi_j \tag{13}$$

In Equation (13), ϕ_j is the basis function at solution point j. If the basis and weighting function are the same, then the process is Galerkin. Both the basis and weighting functions are chosen as Lagrange polynomials in this paper. To provide element coupling flux points are set on element interfaces, and a common Riemann flux is calculated from left and right solution states. In this paper, only the Rusanov [18] interface flux is considered.

2.3. One-Dimensional Problem

As an example of the model in one-dimension, consider the following problem. On a domain from $x = [0, 1]$, let the initial condition consist of two states. A left state $(\rho, u, e, \gamma, p_o)_l = (1.241, 0, 2.753, 1.4, 0)$ for $x \leq 0.5$, and a right state $(\rho, u, e, \gamma, p_o)_l = (0.991, 0, 3.059 \times 10^{-4}, 5.5, 1.505)$ for $x > 0.5$. The domain is partitioned into 200 equally spaced elements, and each element is discretized with three solution points, yielding a P^2 reconstruction. For shock capturing, the same technique discussed in [8] is applied. A three stage Runge-Kutta [19] method is adapted for time integration. The solution for γ and p_o is

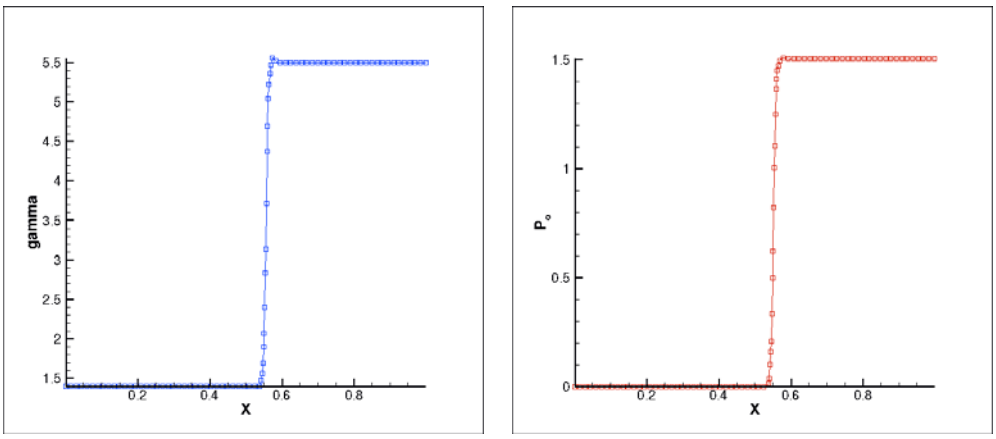

(a) γ solution (b) p_o solution

Figure 2: One dimensional test problem at time $t = 0.1$.

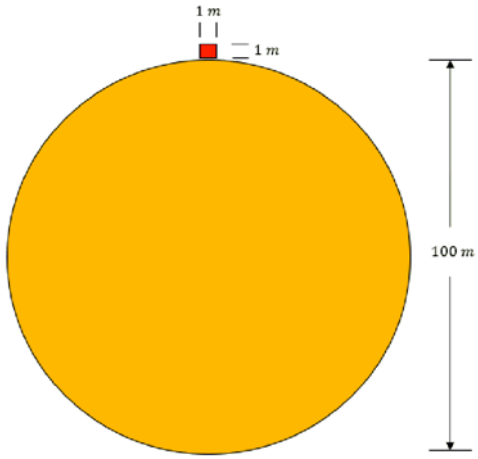

Figure 3: A reference test case with a single kinetic impactor.

shown in figure 2 at a time of $t = 0.1$. The method does an excellent job of capturing the material interface as shown in the figure. In addition, the results compare well with those found in [16]. Application to asteroid deflection is fairly straightforward. The asteroid body, kinetic impactor, and NED each have different γ and p_o variables, which can be tracked throughout the simulation.

3. PROBLEM DESCRIPTION

In this section, the overall problem is defined, as well as the material parameters required. The target body is a circular 100-m diameter asteroid, while the impactor is modeled as a 1×1 m box. There are no porosity effects or varying density with the target asteroid or impactor. The asteroid body is modeled as granite, while the impactor is modeled as aluminum. The constants for γ and p_o are given in Table 1 and taken from [20, 21]. The density is also shown in this table, but for the impactor, it varies from case to case to be presented later. Since our solver demands the speed of sound calculation at element interfaces, it requires a division by the density. Hence, the outside of the asteroid is modeled as air, with a much smaller density than the target or kinetic impactor.

The following problems are investigated in this paper: i) a single, kinetic impactor with varying density and varying shape to investigate the crater depth, ii) a single 5,000-kg kinetic impactor, and iii) five 1000-kg kinetic impactors in parallel or series. The shape of the impactor is varied from a box to a rectangle, with dimensions 0.5×2 m. Figure 4 illustrates both of the multiple kinetic impactor cases.

Table 1: Material parameters

Body	$\rho\,(kg/m^3)$	γ	$p_o\,(Pa)$
Outside	0.1	1.4	0
Impactor	-	3.8	14×10^8
Asteroid	2000.0	2.6	142×10^8

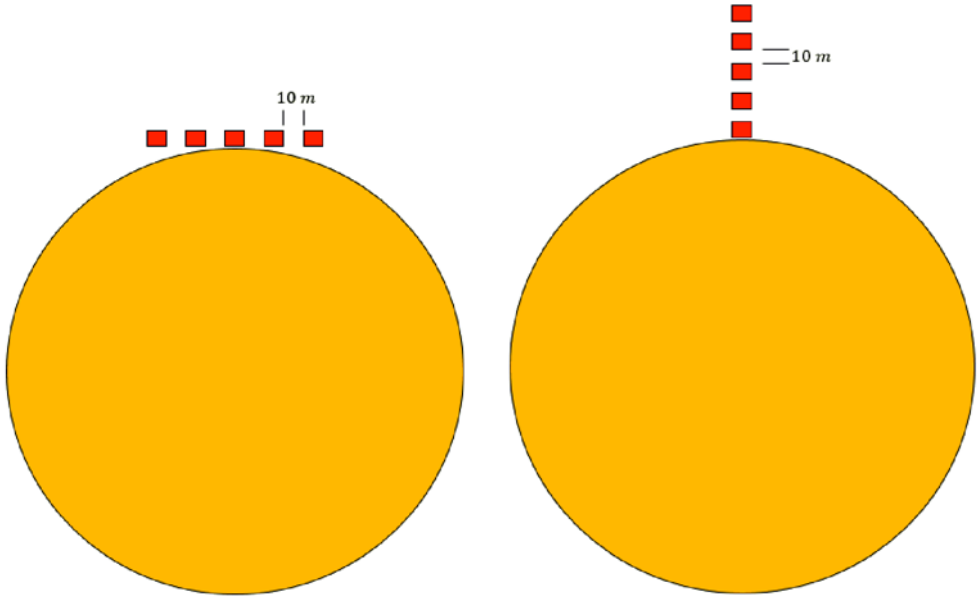

(a) Multiple kinetic impactors in parallel (b) Multiple impactors in series

Figure 4: Illustration of multiple kinetic impactor scenarios.

For the cases of multiple impactors, each impactor remains a 1×1 m box and is spaced equally apart 10 m. At time $t = 0$ seconds, all impactors are assumed to hit, and the kinetic energy transferred to the target body is monitored. The multiple impactors in series is slightly more challenging. Each impactor is spaced 10 m apart, and at time $t = 0$ seconds, the lead impactor hits. It is assumed that the impactors are completely destroyed in these simulations before the following impactor connects. All impactors again are 1×1 m boxes. This paper considers these problems in order to study the overall kinetic energy transferred to the target, the depth of the generated crater, and the predicted damage to the target body.

4. RESULTS

Five test cases are considered in this paper, as follows:

Case 1: Crater depth investigation for a 162-kg impactor and a 600-kg impactor

Case 2: Crater depth investigation for a box- and rectangle-shaped 1000-kg impactor

Case 3: Single 5000-kg impactor

Case 4: Five 1000-kg impactors in parallel

Case 5: Five 1000-kg impactors in series

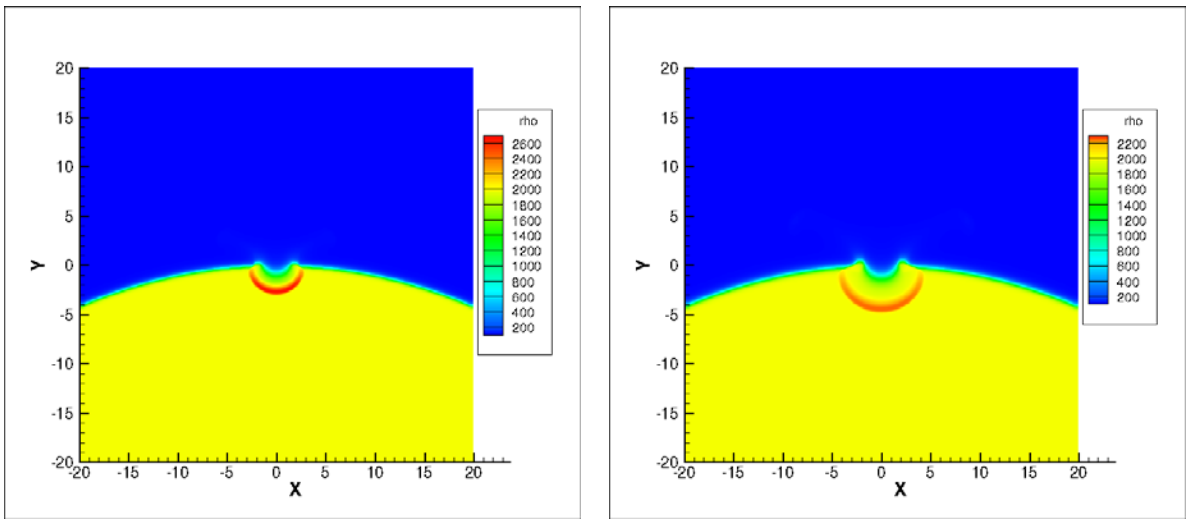

(a) elapsed time = 1.0 ms

(b) elapsed time = 2.0 ms

Figure 5: Case 1A - Asteroid density contours for a case with a single 162-kg impactor.

Table 2: Approximate crater depth for Case 1

Elapsed time	1 ms	2 ms
Case 1A: 162 kg	0.8 m	1.2 m
Case 1B: 600 kg	2.0 m	2.4 m

4.1. Case 1

For this case, we consider two subcases with one kinetic impactor with masses of 162 kg and 600 kg, respectfully. The impactors are initialized with a downward velocity of 11.5 km/s and a corresponding kinetic energy. The damage to the target is comparable between both impactors, as shown in Figures 5 and 6 (the 600 kg impactor appearing to cause slightly more damage). This is because the density of the impactors is much less than that of the target body. Increasing the density will yield higher target damage. Approximate crater depths are recorded at 1 and 2 milliseconds, and are shown in Table 2. It is observed that by increasing the impactor density results in a much deeper crater on the target body, which is expected. The smaller impactor generates a crater size of less than a meter in depth at 1 ms, and it increases by roughly 0.4 m a millisecond later. The larger impactor initially does generate a larger crater, but it also increases by roughly 0.4 m a millisecond later. In this case, most damage occurs immediately when the impactor connects with the body and imparts kinetic energy. Little damage propagation is observed after this occurs. In addition, the errors in momentum were checked at the final simulation time, to verify the conservation of linear momentum. These momentum errors are normalized with the initial momentum contained in the impactor. For the 162 kg case at 2 ms simulation time, the error in x-momentum was 9.12×10^{-13} and the error in y-momentum was 1.37×10^{-9}. Similar errors were seen in the 600 kg impactor and in the following tests.

4.2. Case 2

A different geometry for the impactor is considered in this test case. The mass of the impactor is kept at 1,000 kg, and two types of geometries are considered. One geometry is a box of 1×1 m (Case 2A), while the other is a rectangle of 0.5×2 m (Case 2B) with $D < L$. In both test cases, each impactor is set with a downward velocity of 10 km/s and a corresponding kinetic energy. Figures 7 and 8 show the results at two separate times for the box and rectangular impactors, respectfully. The rectangular impactor crater is roughly 50% larger than the box impactor crater at 1 millisecond of simulation time. In addition, the rectangular impactor allows for more surface area to retain more energy from the NED to be integrated into the crater. The box impactor does generate a stronger shock, but the rectangular

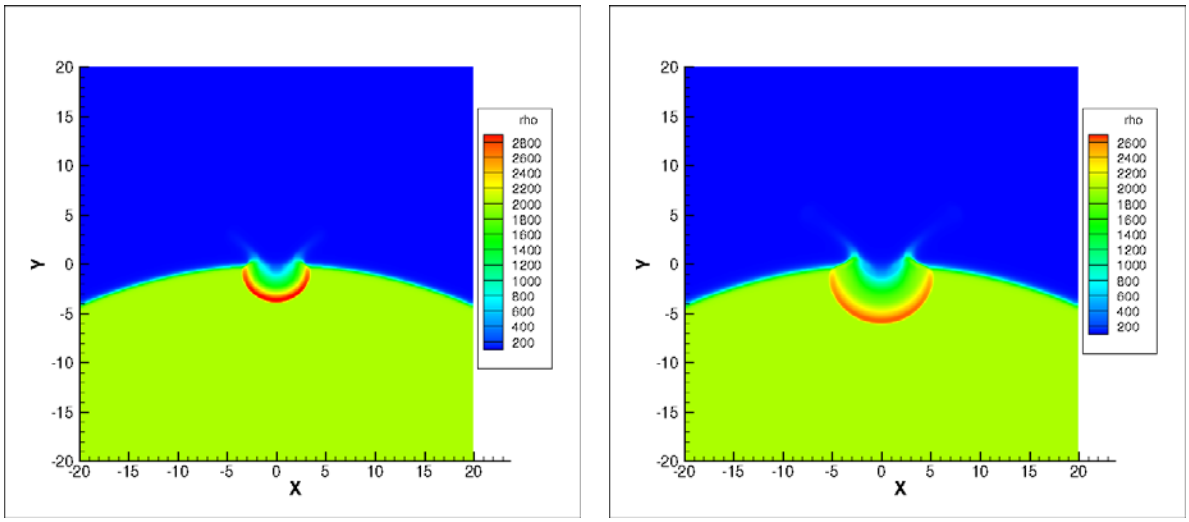

(a) elapsed time = 1.0 ms (b) elapsed time = 2.0 ms

Figure 6: Case 1B - Asteroid density contours for a case with a single 600-kg impactor.

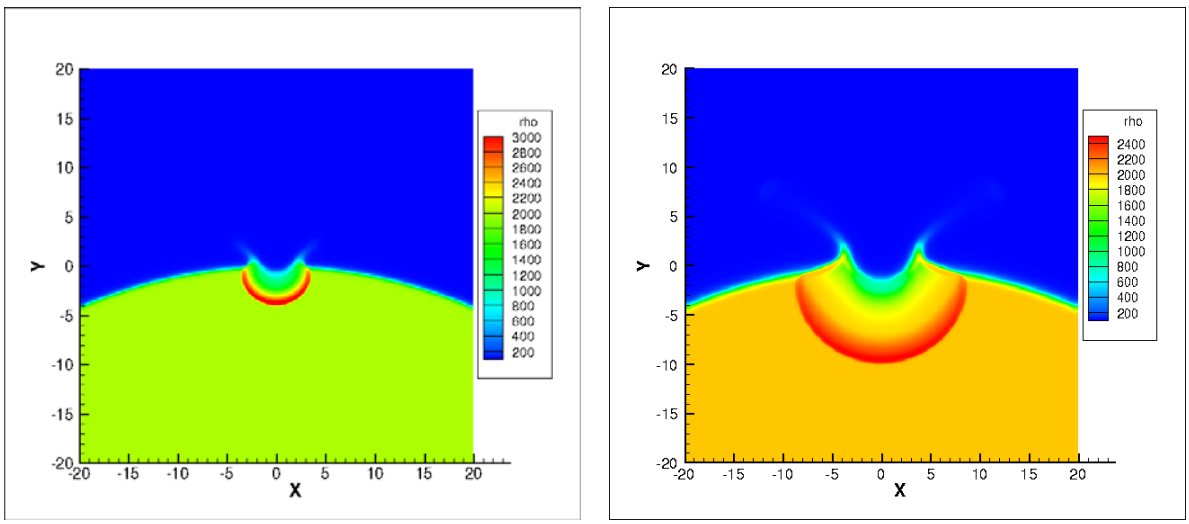

(a) elapsed time = 1.0 ms (b) elapsed time = 4.0 ms

Figure 7: Case 2A - Asteroid density contours for a case with a single 1,000-kg box-shaped impactor with $L/D = 1$.

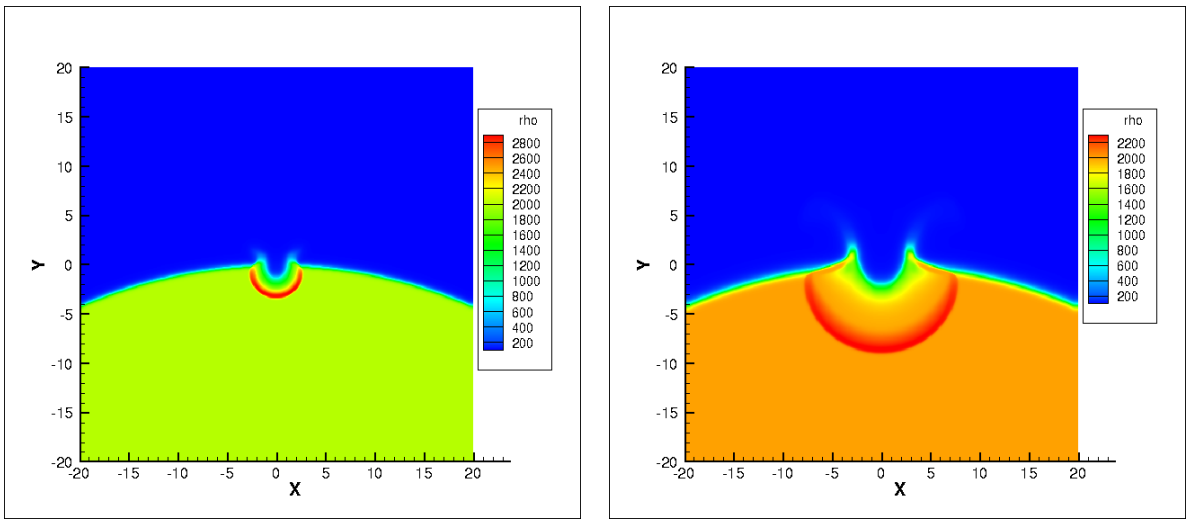

(a) elapsed time = 1.0 ms

(b) elapsed time = 4.0 ms

Figure 8: Case 2B - Asteroid density contours for a case with 1,000-kg rectangular impactor with $L > D$.

impactor will be better for the HAIV concept, generating a slightly deeper crater and yielding a more enclosed surface for improved coupling of energy from the NED.

4.3. Case 3

In this case, an extremely dense impactor is used, with a mass of 5,000 kg. The impactor is initialized with an initial downward velocity of 10 km/s and corresponding kinetic energy. The kinetic energy imparted to the target is monitored, and will be shown later. Figure 9 shows the density contours at elapsed times of 1 and 4 milliseconds. The heavy impactor seems to generate a substantial amount of upward moving material at 4 milliseconds, making crater prediction difficult. It should be noted that the initial shock wave into the body is much stronger than that of the 162- or 600-kg impactors (roughly 15% stronger).

4.4. Case 4

In this test case, an array of five impactors is considered. Refer to Section 3 for the geometry of the problem. At the initial time ($t = 0$), all five impactors strike the target. All impactors have the same initial kinetic energy, traveling downward at 10 km/s. It is important to note that the lead impactor hits perpendicular to the body, while the remaining four are slightly off from perpendicular. This does have an important effect on the transferred kinetic energy. Density contours for the array of impactors is shown in Figure 10 at four elapsed times. A nearly symmetric set of shock waves is present in the simulation (nearly symmetric because in the initial condition, exactly 10 m separation between the impactors could not be set). One important issue addressed here is the amount of kinetic energy transferred to the target per impactor. The kinetic energy is monitored by using the following equation:

$$E_k = \frac{1}{\Gamma}\int_{\Gamma}\rho\frac{\mathbf{v}\cdot\mathbf{v}}{2}d\Omega \tag{14}$$

where Γ is the size of the target body and $\mathbf{v}$ is the velocity vector. For the five impactors, let the lead impactor be impact 1, the impactor 10 meters to its right impact 2, and the impactor 20 meters to its right impact 3. It is observed in Figure 11, that the further away from perpendicular, the less kinetic energy transferred into the target body. From impact 1 to impact 3, roughly 45% of the possible coupled kinetic energy is lost into the surrounding space. In order to minimize this amount, the impactors should hit perfectly perpendicular with the body, which is nearly impossible in realistic scenarios. Hitting perpendicular with each impactor would require detailed surface information of the target, and could require a large change in the velocity vector of the impactor.

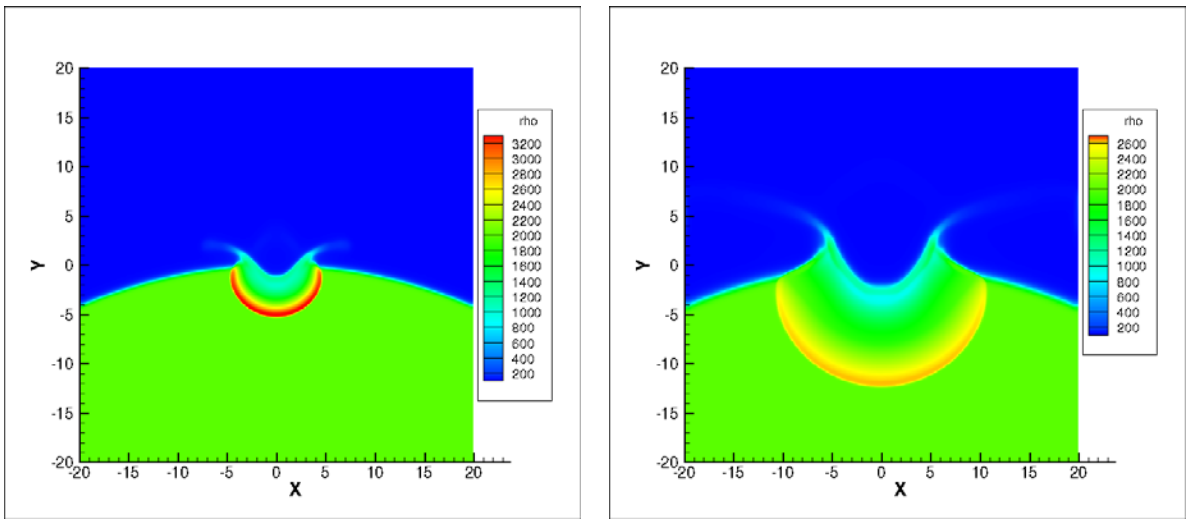

(a) elapsed time = 1.0 ms

(b) elapsed time = 4.0 ms

Figure 9: Case 3 - Asteroid density contours for a case with a single 5,000 kg impactor.

However, the simulation results (at t = 8 msec) indicate that multiple impactors in parallel appear to cause significant damage to a wide area of the target body. The generated shock waves cover a wide distance through the body, and will probably aid in effective pulverization/fragmentation. This type of disruption may become more effective for porous targets, which will be examined in detail in future work.

4.5. Case 5

Rather than an array of impactors in parallel, an array of multiple impactors in series is considered here. Again, the geometry of this problem is discussed in Section 3. At the initial time of t = 0, the lead impactor makes contact with the target. Each impactor is traveling downward at 10 km/s, meaning that after an impactor hits, a follower impactor will make contact roughly 0.1 milliseconds after. Results for five different elapsed times are shown in Figure 12. Each subfigure illustrates the density contours 1 millisecond after the impact. For example, Figure 12 (c) is 1 millisecond after the third impactor has struck the target, or total time of 3 milliseconds. This case has complex shock wave interactions within the body, where the leading shock is strengthened after each subsequent kinetic impact. A benefit of this approach is the depth of the crater, which at 5 milliseconds is roughly 5 meters. Hence, one possible solution to effect a deeper subsurface explosion is to use mutliple impactors in series prior to a subsurface nuclear explosion.

4.6. Comparison of Results

A comparison of Cases 3, 4, and 5 is of practical significance. The kinetic energy of the cases is plotted and discussed here. Figure 13 (a) illustrates the total kinetic energy imparted to the body from a single 1,000 kg impactor (1,000 kg - Impact 1), a single 5,000 kg impactor (5,000 kg - Impact 1), and and array of impactors (1,000 kg - Impact 5). From this figure, it is apparent that five 1,000 kg impactors in a parallel couple less energy than one 5,000 kg impactor. In fact, the multiple impactors impart 50% less energy into the circular target. Figure 13 (b) shows the multiple impactors in series, which couple more energy than the parallel array of impactors (roughly 15% more), but is still less effective than the single heavy impactor. Of course, the multiple impactors in series requires more time to couple the energy as well. Since each impactor is 10 meters behind its leader and the velocity is 10 km/s, coupling the total kinetic energy requires five times the time as an array of impactors or a single impactor. However, the multiple impactors in series does offer a possible solution to coupling more energy from the NED to the target body. By increasing the depth of the crater, the amount of coupled energy from an NED will increase, improving the overall damage from the NED, and effectiveness of the HAIV mission concept.

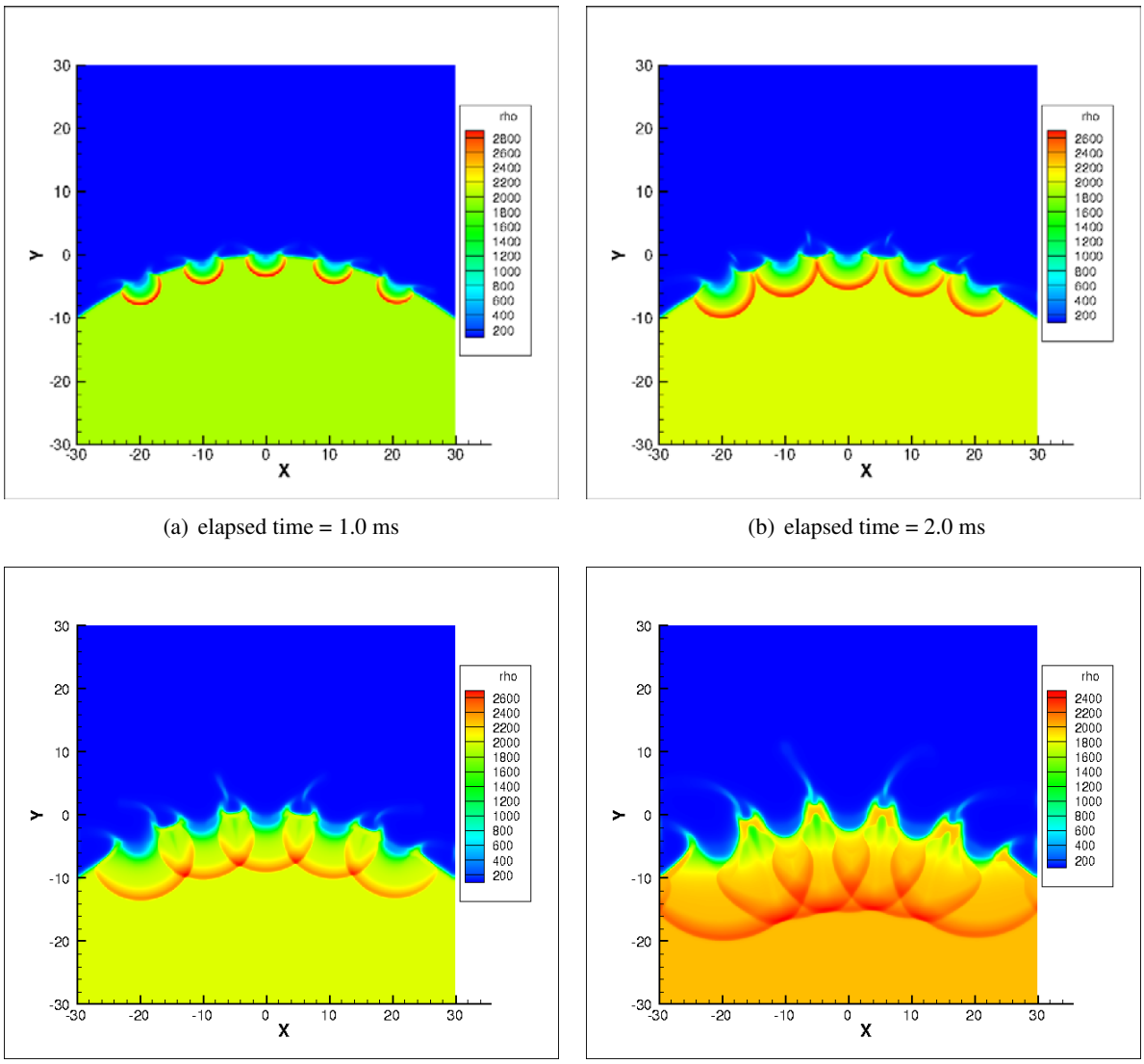

(a) elapsed time = 1.0 ms

(b) elapsed time = 2.0 ms

(c) Time 4.0 ms

(d) elapsed time = 8.0 ms

Figure 10: Case 4 - Asteroid density contours for a case with five 1,000-kg impactors in parallel.

4.7. HAIV Concept

Preliminary results for the HAIV concept are presented here. In order to improve the effectiveness of a subsurface nuclear explosion, multiple kinetic impactors in series (as discussed in Case 5) was simulated to generate a deeper crater. Figure 14 (a) shows the initial crater generated by the impactors at detonation time of $t = 0.0$. At this time, a 100-kt NED is placed inside the crater. This figure illustrates the density contours for multiple times after detonation has occurred. Continued research is required for the HAIV mission concept. Radiation (e.g., soft x-ray) is not considered in the mathematical model in this paper. Furthermore, the stiffened equation of state does not accurately model the materials at such high temperatures, and a new equation of state must be investigated.

5. CONCLUSIONS AND FUTURE WORK

In this paper, the effectiveness of multiple kinetic impact approaches as well as the HAIV concept was investigated using new GPU-accelerated computational tool. Lightweight impactors, with density much less than the target, produce relatively small craters (approximately 1 - 2 meters in depth) in a short elapsed time. The multiple impactors in parallel does have the capability to inflict high damage

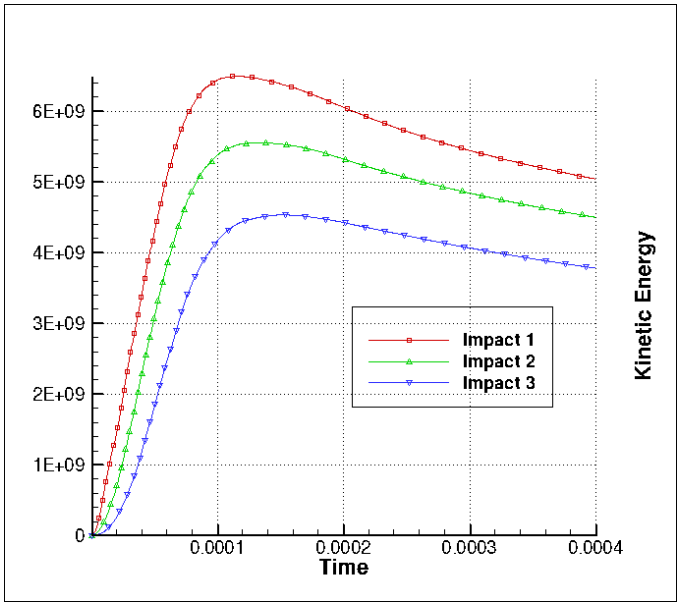

Figure 11: Total kinetic energy for three impactors in Case 3.

in a wider area, providing an non-nuclear option for soft or porous targets. A serial array of multiple impactors has been shown to be very effective for deep penetration. Not only does it couple more kinetic energy than the parallel array of multiple impactors, but it also increases the crater depth, which will increase the efficiency of the HAIV concept. In this study, only a circular target with constant density was considered. Future work must include more realistic asteroid bodies. Additionally, the density of the targets should be varied, including porosity, to further investigate non-nuclear multiple kinetic impact options as well as the HAIV concept. A new equation of state is desired, as the current one implemented does not hold for the high temperatures and pressures associated with the problem. Finally, the effect of radiation (e.g., a soft x-ray) should be considered, as its effect on the asteroid body is currently not included in our simulations.

References

[1] National Research Council. *Defending Planet Earth: Near-Earth Object Surveys and Hazard Mitigation Strategies.* 2010.

[2] J. Sanchez, M. Vasile, and G. Radice. On the consequences of a fragmentation due to a NEO mitigation strategy. IAC-08-C1.3.10, Glasglow, United Kingdom, September 29 - October 3 2008. 59th International Astronautical Congress.

[3] B. Wie. Hypervelocity nuclear interceptors for asteroid disruption. *Acta Astronautica*, 90:146-155, 2013.

[4] A. Pitz, B. Kaplinger, G. Vardaxis, T. Winkler, and B. Wie. Conceptual design of a hypervelocity asteroid intercept vehicle (HAIV) and its flight validation mission. *Acta Astronautica*, 94:42-56, 2014.

[5] B. Barbee, B. Wie, M. Steiner, and K. Getzandanner. Conceptual design of a flight demonstration mission for a hypervelocity asteroid intercept vehicle. *Acta Astronautica*, Vol. 106, 2015, pp. 139-159.

[6] B. Kaplinger, P. D. Premaratne, C. Setzer, and B. Wie. GPU-Accelerated 3D modeling and simulation of a blended kinetic impact and nuclear subsurface explosion. *AIAA*, (2013-4548), 2013.

[7] National Academy of Sciences. *Effects of Nuclear Earth-Penetrator and Other Weapons.* 2005.

[8] B. J. Zimmerman and B. Wie. Computational validation of nuclear explosion energy coupling models for asteroid fragmentation. *AIAA*, (2014-4146), 2014.

[9] Bassi F, Rebay S. High-order accurate discontinuous finite element solution of the 2D Euler equations. J Comput Phys 1997;138:251-285.

[10] Baumann CE, Oden TJ. A discontinuous hp finite element method for the Euler and Navier-Stokes equations. J Numer Meth Fluids 1999;31(1):79-95

[11] Cockburn B, Shu CW. The Runge-Kutta discontinuous Galerkin method for conservation laws V: multidimensional systems. J Comput Phys 1998;141:199-224.

[12] M. Hoffmann, C-D. Munz, and Z. J. Wang. Efficient implementation of the CPR formulation for the Navier-Stokes equations on GPUs. *ICCFD*, 7-2603, 2012.

[13] B. J. Zimmerman and Z. J. Wang. The efficient implementation of correction procedure via reconstruction with GPU computing. *AIAA*, (2013-2692), 2013.

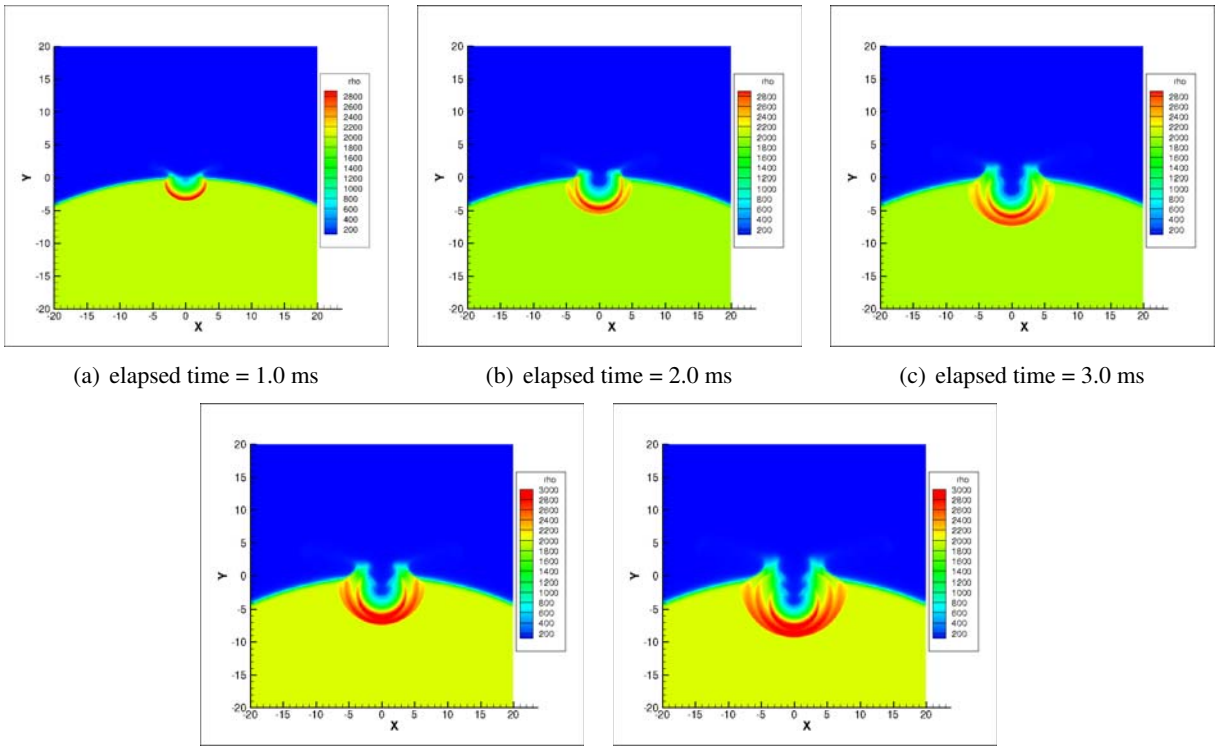

(a) elapsed time = 1.0 ms (b) elapsed time = 2.0 ms (c) elapsed time = 3.0 ms

(d) elapsed time = 4.0 ms (e) elapsed time = 5.0 ms

Figure 12: Case 5 - Asteroid density contours for a case with five 1,000-kg impactors in series.

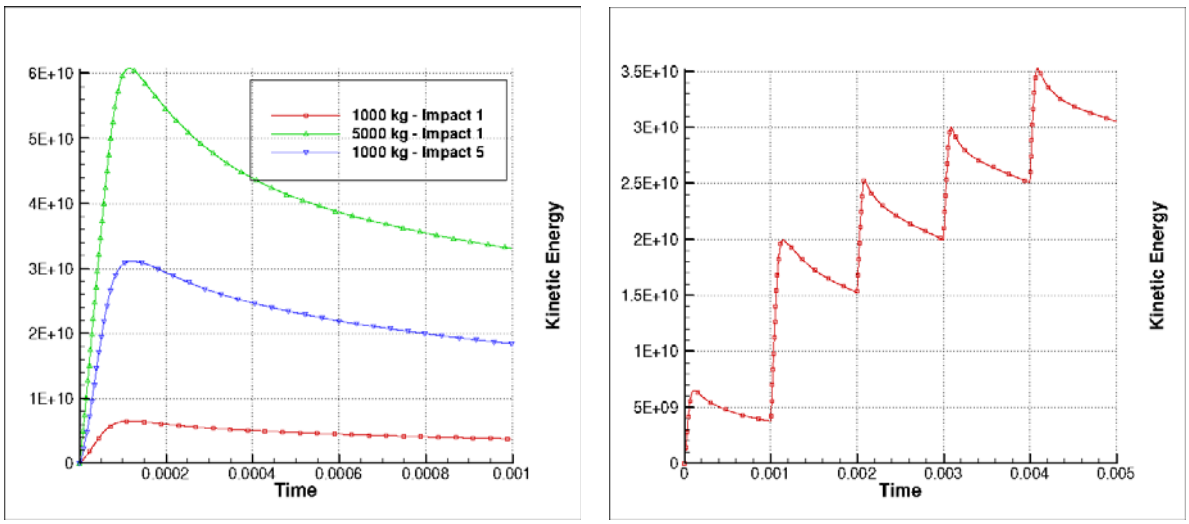

(a) Single and parallel array of impactors (b) Multiple impactors in series

Figure 13: Total kinetic energy coupled to the target.

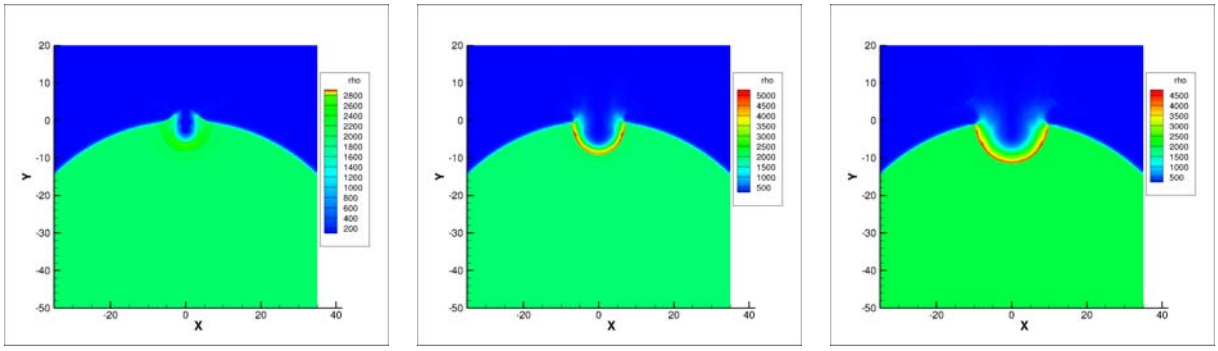

(a) elapsed time = 0.0 ms (b) elapsed time = 0.05 ms (c) elapsed time = 0.1 ms

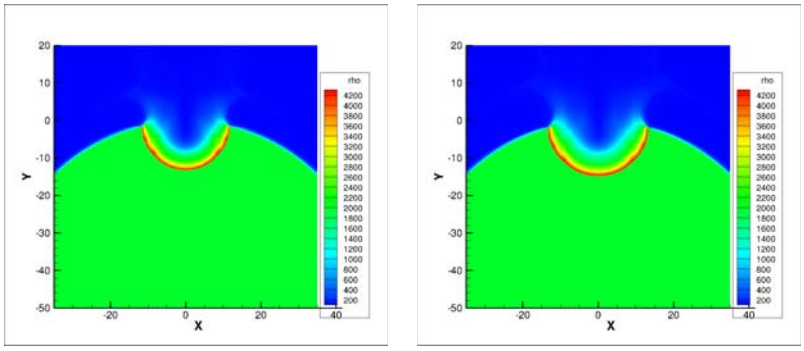

(d) elapsed time = 0.15 ms (e) elapsed time = 0.2 ms

Figure 14: Simulation result for the HAIV concept of blending a kinetic impact and a subsurface nuclear explosion.

[14] R. F. Prater. Hypervelocity impact - material strength effects of crater formation and shock propagation in three aluminum alloys. *PhD Thesis*, AFML-TR-70-295, 1970.

[15] K. S. Holian. T-4 handbook of material properties data bases. Tech. Rep. LA-10160-MS, Los Alamos National Laboratory, 1984.

[16] K. Shyue. An efficient shock-capturing algorithm for compressible multicomponent problems. J. Comput. Phys. 1998;142:208-242.

[17] O. C. Zienkiewicz and R. C. Tayler. *The Finite Element Method The Basics.* 2000.

[18] V. V. Rusanov. Calculation of interaction of non-steady shock waves with obstacles. *Journal of Computational Mathematical Physics*, USSR(1), 1961.

[19] C. W. Shu. Total-variation-diminishing time discretizations. *SIAM Journal on Scientific and Statistical Computing*, 9, 1988.

[20] R. Saurel, O. Le Metayer, J. Massoni, and S. Gavrilyuk. Shock jump relations for multiphase mixtures with stiff mechanical relaxation. *Shock Waves*, 2007;16:209-232

[21] R. Saurel and R. Abgrall. A simple method for compressible multifluid flows. SIAM J. Sci. Comput. 21;3:1115-1145. 1999.